Adsorption Technique for Color Removal from Aqueous Solution using Nano NiO as Adsorbent

Omar Sadiq Ali[1*] 🆔✉ **and Dunya Edan AL-Mammar[2]** 🆔✉

[1,2]Department of Chemistry, College of Science, University of Baghdad, Baghdad, Iraq.

*Corresponding Author.

Abstract

In the present study, nickel oxide nanoparticles (NiO-NPs) were synthesized using the aqueous extract of two leaf plants, Allium porrum (Leek) NiO-P and Apium graveolens (Celery) NiO-G, as reducing agents. The synthesized NiO-NPs were utilized as adsorbents to remove Biebrich Scarlet (BS) dye from water using the adsorption technique. The NiO-P and NiO-G surfaces were characterized using Fourier transform infrared (FTIR), X-ray diffraction (XRD), atomic force microscopy (AFM), scanning electron microscopy (SEM), and Brunauer-Emmett-Teller (BET). The batch adsorption experiments were achieved to explore the optimum conditions for the adsorption of BS dye onto the synthesized NiO-NPs, such as NiO-NPs dosage, initial concentration of BS, contact time, temperature, and pH. The equilibrium data of BS adsorption on NiO-P and NiO-G surfaces best fitted the Langmuir isotherm model. Thermodynamic data such as $\Delta G°$, $\Delta H°$, and $\Delta S°$ were also estimated. The adsorption of BS dye onto NiO-P and NiO-G surfaces is a spontaneous and endothermic process. The adsorption rates were calculated by pseudo-first-order (PFO) and pseudo-second-order (PSO) kinetics models, and it was obtained that the correlation coefficient R2 for PSO was in the range of 0.9762-0.9971 and 0.9408-0.9966 for NiO-P and NiO-G, respectively. Furthermore, the qe cal values for PSO are almost in agreement with the experimental qe exp at all temperatures. As a result, the rate mechanism is well explained by the pseudo-second-order model (PSO).

Keywords: Leek, celery, kinetic, Biebrich Scarlet, nickel oxide.

1. Introduction

Water is the most important renewable resource. Color pollutants are easily detected in water, even at low concentrations. In addition, minor dyes in water "may be carcinogenic and toxic to humans and aquatic organisms" and can lead to allergic dermatitis or skin irritation. The primary waste sources are agricultural waste, untreated wastewater, industrial pollution, and industrial effluent [1]. Dye removal from the manufacturing sector, including the food, textile, printing, and leather industries, all contribute to a severe environmental problem [2].

Therefore, before being released into any freshwater body, textile wastewater needs to go through a number of treatment procedures, including physical, chemical, and biological [3].

The adsorption technique is a physical or chemical bonding arising from the bonding forces between atoms, molecules, or ions of a particular substance called an adsorbate, which may be liquid, gaseous, or porous solid surfaces called an adsorbent [4]. This technique has lately gained popularity among academics because of its excellent efficiency and practical cost for removing color from wastewater [5].

Nanoparticles (NPs) have become more well-known in recent years as a result of their unique attributes, which include a large surface area compared to their small size, chemically reactive sites, competitive binding sites, excellent chemical stability, and an optically active surface [6]. Nickel oxide NPs (NiO-NPs) are a promising material employed in various applications, including catalysis, electrochromic films, and supercapacitors [7]. Several techniques have been used for the preparation of NiO-NPs, such as Physical vapor deposition (PVD), colloidal or wet chemical route, sol-gel method, and green chemistry method. The most widely used method for synthesizing NPs is the green method, which is considered low-cost, simple, non-toxic, and eco-friendly [8]. An exceptional source for the creation of NPs, plant bio-variations offer a range of biological characteristics. It is quite easy to get the plant leaf extract for use, and it contains several metabolites that work as reducing and stabilizing agents to create NPs. This study attempted to synthesize NiO-NPs using Allium porrum and Apium graveolens leaf extracts as reducing agents to synthesize NiO-P and NiO-G NP samples. The synthesized NPs were utilized as adsorbents to remove BS dye from water using the adsorption technique.

2. Materials and Methods

2.1 Materials

Nickel (II) chloride hexahydrate $NiCl_2.6H_2O$ from Thomas Baker (99%), sodium hydroxide, pure ethanol (99%), and Biebrich Scarlet dye purchased from BDH (99%) were used in this work.

2.2 Preparation of adsorbate

Biebrich scarlet (BS) dye, or acid red 66, is an anionic dye with the chemical formula $C_{22}H_{14}N_4Na_2O_7S_2$. Its IUPAC name is sodium-6-(2-hydroxynaphthylazo)-3,4-azodibenzene sulfonate. It is a water-soluble dye with a molar mass of 556.48 g/mol, a maximum wavelength of 505 nm, and a C.I. number of 26905 [9]. **Figure 1** depicts the dye's chemical structure.
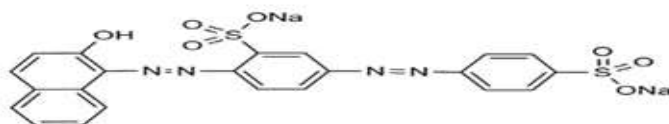
Figure 1. Chemical structure for BS dye.

To prepare 1000 ppm of BS dye as adsorbate, one gram of BS dye powder was dissolved in 1000 mL of distilled water, and then the stock solution was diluted to the following concentrations: 10, 20, 30, 40, and 50 mg/L. The absorbance of the solution was determined using a UV-Vis spectrophotometer.

2.3 Synthesis of NiO-P NPs using allium porrum

At first, the aqueous extract was prepared by washing 30 g of the Allium porrum with water several times to remove any dust, blending it with 300 ml of distilled water in a blender, and placing it in a conical flask at 80°C while stirring for 50 minutes. It was then cooled, filtered, and stored in the refrigerator for later use. To prepare the NiO–P sample, 30 mL of plant extract was added to a mixture of 4 g $NiCl_2.6H_2O$ and 100 mL distilled water, stirring for 30 min at 70 ˚C. A few drops of 0.1 M sodium hydroxide were added in order to make the pH equal to 10. The precipitate was filtered using Whatman No. 1 filter papers, then left at room temperature for 24 hours, followed by filtration and washing with distilled water and ethanol in a ratio of 3:1 to remove unreacted particles, and heating in an oven for one hour at 110˚C to form NiO–P as green powder.

2.4 Synthesis of NiO-G NPs using apium graveolens

About 20 g of plants were placed in a 250 mL conical flask with 200 mL of distilled water and heated to 80 °C for 50 minutes with stirring, then cooled and filtered [10]. The filtrate material (yellow) was stored in the refrigerator. To synthesize the NiO-G sample, 2 g of nickel chloride hexahydrate solution is dissolved in 100 mL of distilled water, then heated to 70 °C for 30 minutes with the addition of 50 mL of leaf extract. Green gel precipitates appeared when 0.1 M NaOH was added to the mixture and left for one night. Then, it was separated by centrifugation for 10 minutes at 3000 rpm. The sediments were washed with distilled water and pure ethanol in a 3:1 ratio. The resulting sediment was dried and calcined in the oven at 110°C for 1 hour to obtain a dark green precipitate.

2.5 Characterization

The NiO-NPs samples were characterized by using several techniques, such as the Fourier transform infrared spectroscopy (FTIR) Shimadzu model in the region 4000-400 cm^{-1}, X-ray diffraction (XRD) pattern investigated with anode Cu k (λ=0.154 λ=0.154nm) using X'pert Pro2021, the atomic force microscopy (AFM) model (NaioAFM-Switzerland), and scanning electron microscopy (SEM) instrument type (Inspect f50-Fei Co.-Netherlands) to identify the surface morphology. Brunauer-Emmett and Teller (BET) analysis was carried out using Micrometrics Gemini VII (Germany). The UV-Vis-Visctrophotometer model (Shimadzu) was used to determine the absorption wavelength for the dye.

2.6 Adsorption experimental

The adsorption of BS dye onto NiO-NPs samples was studied using batch methods. Studying the impact of the BS dye concentration was carried out by using different concentrations from 10 to 50 mg/L with an adsorbent weight of 0.05 g/25 mL of BS dye and an adsorption time of 40 min. The residual BS dye concentration was determined using a UV-Vis spectrophotometer. The influence of the adsorbent weight was determined by changing the amount of NiO-NPs from 0.01 to 0.1 g/25 mL of 10 mg/L BS dye concentration in a 100 mL conical flask. The effect of adsorption time was studied at 298 K with an adsorbent weight of 0.05 g/25 mL in a dye solution with a concentration of 10 mg/L at agitation times between 5 and 60 minutes. The effect of pH solutions was tested in the 2.2–10.3 pH range by adding a few drops of either 0.1 M NaOH or 0.1 M HCl.

The following formulas were used to compute the removal percentage (R%) for BS dye and the quantity of adsorbed dye (qe) mg/g [11].

$$R\% = [(C_i - C_e)/C_i] \times 100 \tag{1}$$

$$q_e = [(C_i - C_e)/C_e] \times {}^V\!/_m \tag{2}$$

Where Ce (mg/L) is the dye concentration at equilibrium, Ci (mg/L) is the initial dye concentration, m (g) is the adsorbent dosage, and V (L) is the working solution volume.

2.7 Equilibrium isotherm models

The adsorption of BS dye from the aqueous solution onto NiO-NPs surfaces were assessed by two adsorption isotherm models, namely; Langmuir and Freundlich. Langmuir model described the homogenous, uniform adsorption. This model is represented in the following linear equation:

$$\frac{C_e}{q_t} = \frac{1}{K_L \cdot q_m} + \frac{C_e}{q_m} \tag{3}$$

The effectiveness of adsorption was calculated using the dimensionless constant or separation factor R_s, which was estimated using the following equation [12]:

$$R_s = \frac{1}{1 + K_L \cdot C_i} \tag{4}$$

Where C_i and C_e (mg/L) are the starting and equilibrium concentrations of the BS dye respectively, q_e refers to the equilibrium amount of the substance adsorbed per gram of the adsorbent (mg/g), q_m is the maximum monolayer coverage (mg/g), and K_L is the Langmuir isotherm constant (L/mg). The values of K_L and q_m are estimated from the linear plot between C_e/q_e against C_e. The values of R_s specify that the adsorption was irreversible R=0, favorable ($0 < R_S < 1$), linear $R_s=1$, or unfavorable $R_s > 1$.

The Freundlich model describes heterogeneous surfaces that have different values of diffusion energy. The linear equation is written as [13].

$$\ln q_e = \ln K_{fr} + \frac{1}{n_f} \ln C_e \tag{5}$$

Where k_{fr} is the Freundlich constant related to the adsorption capacity (mg/g $(L/mg)^{-1/n}$) and n_f is the adsorption intensity, these values were calculated from the intercept and slope of the linear relation between $\ln q_e$ and $\ln C_e$.

2.8 Thermodynamic studies

Thermodynamic properties are studied at different temperatures in order to investigate the effect of temperature on the adsorption process, either spontaneously or randomly. Thermodynamic parameters were calculated by the equations [14].

$$\Delta G^\circ = - RT \ln K_{eq} \tag{6}$$

$$K_{eq} = q_e/C_e \tag{7}$$

$$\Delta G^\circ = \Delta H^\circ - T \Delta S^\circ \tag{8}$$

Where Keq equilibrium constant of the adsorption, Ci and Ce (mg/L) are the initial and equilibrium concentrations of the adsorbate, respectively. V: volume of the solution (L); m (g): weight of the adsorbent. R: universal gas constant (8.314 J.mol/K) and T(K) absolute temperature. The values of ΔS° and ΔH° can be obtained from the intercept and slope when ln Keq is plotted against 1/T according to the Van't Hoff equation [15].

$$\ln K_{eq} = \Delta S^\circ/R - \Delta H^\circ/RT \tag{9}$$

2.9 Adsorption kinetic studies

Adsorption kinetics are used to estimate the reaction pathways and the equilibrium time. Different kinetic models are applied to describe the adsorption process [16]. The pseudo-first-order (PFO) model was applied to liquid and solid systems based on solid capacitance [17]. The equation expressed it.

$$\ln(q_e - q_t) = \ln q_e - K_1.t \tag{10}$$

Where qe, qt are the adsorption capacity at equilibrium time and the adsorbed amount of adsorbate at time (mg.g^{-1}), respectively, k_1 is the PFO rate constant (min^{-1}) for the adsorption process, and t is the time (min). From the graph between ln (qe-qt) versus t, the values of k_1 and qe [18]. The kinetic rate equation for the pseudo-second-order (PSO) model is given as [19].

$$\frac{t}{q_t} = \frac{1}{k_2\,q_e{}^2} + \frac{t}{q_e} \tag{11}$$

Where k_2 is the equilibrium rate constant of the PSO equation (g/mg.min), k_2 and q_e can be estimated from the intercept and the slope of plotting t/qt versus t.

3. Results and Discussion

3.1 Characterization of NiO−NPs

3.1.1 Fourier transform infrared spectroscopy (FTIR)

The FTIR spectrum for NiO-NPs samples is shown in **Figure 2**.
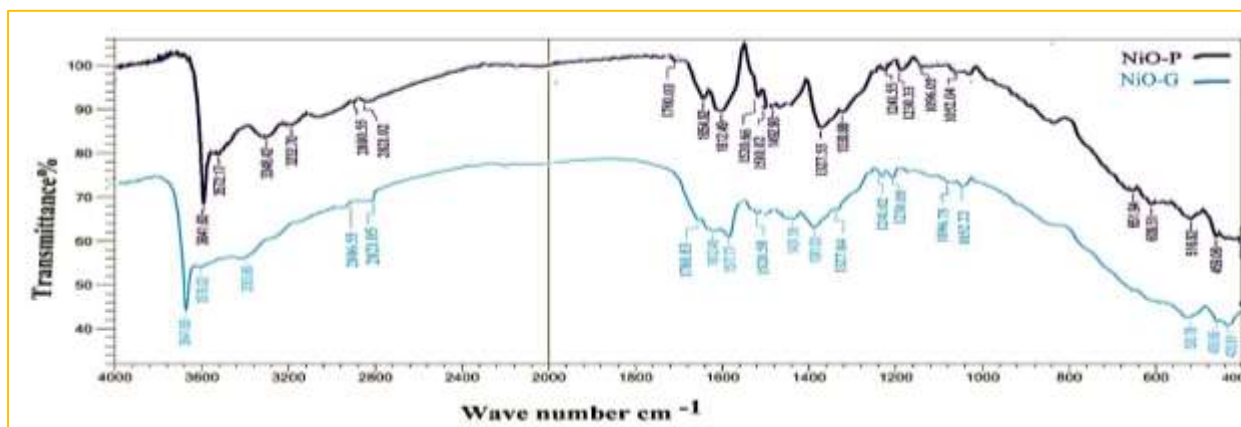
Figure 2. The FTIR transmission for NiO−P and NiO−G samples.

As seen in **Figure 2**, the samples have the same broadband between 3641-3000 cm^{-1}, which is associated with the hydroxyl group as a result of the moisture of the water on the NiO surface. It may also be related to the N-H band, which overlaps the O-H band [20]. It is possible to observe the location of the C−H and C−C groups responsible for aromatic expansion vibrations in the aromatic carbonyl at peaks 2886 cm^{-1} and 2880 cm^{-1}, respectively. The absorption peak at 1780–1510 cm^{-1} corresponds to the C=O and C=C stretching vibrations in the aromatic region. The peaks 1654–1612 cm^{-1} are for the C=C group of aromatic rings, which are specific to the plant extract. The bands 1492–1431 cm^{-1} show the CH$_2$ group, while the peaks 1381–1300 cm^{-1} are for the CH$_3$ group; the peak at 1241 cm^{-1} is among others characteristic of the O=C-O-C ester bond present in the plant extract; and the absorption peaks appear at 1096–1052 cm^{-1} for the C-O bond stretch vibration of alcohols and carboxylic acid groups. The FTIR spectra for metal-oxygen bands show a region of 400–800 cm^{-1}. Thus, the peak at 651 cm^{-1} is associated with the Ni-O-H stretching bond, and the other peaks (520–435 cm^{-1}) are assigned to the NiO bending vibrations.

3.1.2 The X-Ray diffraction (XRD)

The XRD was used to evaluate the crystal and structural properties of the produced samples. **Figure 3 (a,b)** shows the XRD patterns of NiO-NPs samples. All sample peaks agreed with both the Miller indices and the reference cards. The position of peaks for NiO-P and NiO-G corresponds to the same last Miller indices 111, 200, 220, 311, and 222, along with the rhombohedral cubic crystal structures at $2\theta°$ (37˚, 43˚, 63˚, 75˚, and 79˚) and the reference card (JCPDS card No. 00-044-1159). The values of average crystal size (D) for NiO-P and NiO-G samples were calculated using X'Pert HighScore software and found to be 21.34 and 25.72 nm, respectively. The difference in crystal size between the samples is a result of the presence of phytochemicals on their surfaces, which leads to the reduction of D and increases the effectiveness of the adsorption of BS dye.
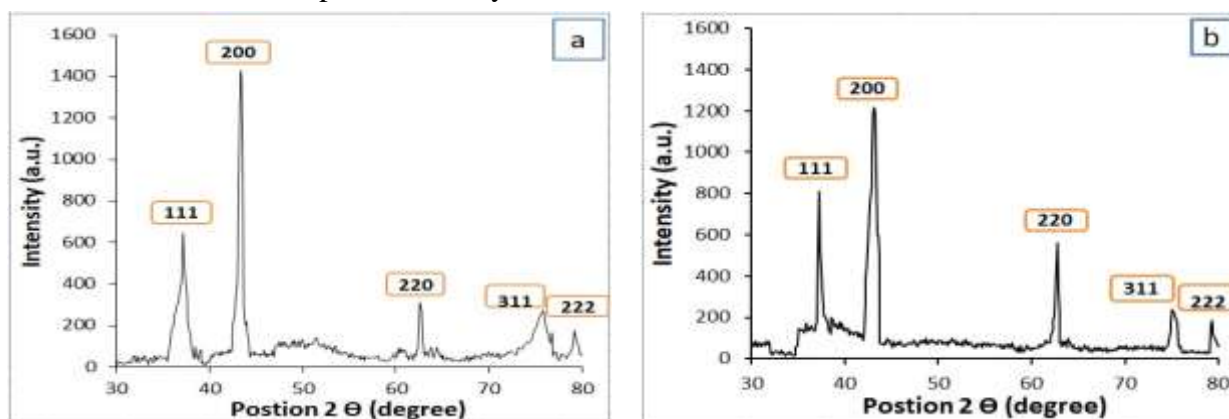
Figure 3. The XRD patterns for (a) NiO-P (b)NiO-G.

3.1.3 Atomic force microscopy (AFM)

The AFM technique was utilized to collect the data on the average diameter of the grains, volume, and **3D Images** of granules. **Figure 4 (a,b)** depicts a typical surface and granularity cumulating distribution for NiO-NPs samples. The average diameters of NiO-P and NiO-G are 87.80 and 88.35 nm, respectively, while the average volumes of the particles are 2.04 and 5.02 nm^3. The AFM investigation of NiO-NPs revealed that the size and shape of the NiO-NPs were significantly impacted by the change in synthesis techniques due to the presence of phytochemical substances. The difference between surfaces is the average diameter and volume of the particles; the lower the ratio, the higher the surface's effectiveness in dye adsorption.
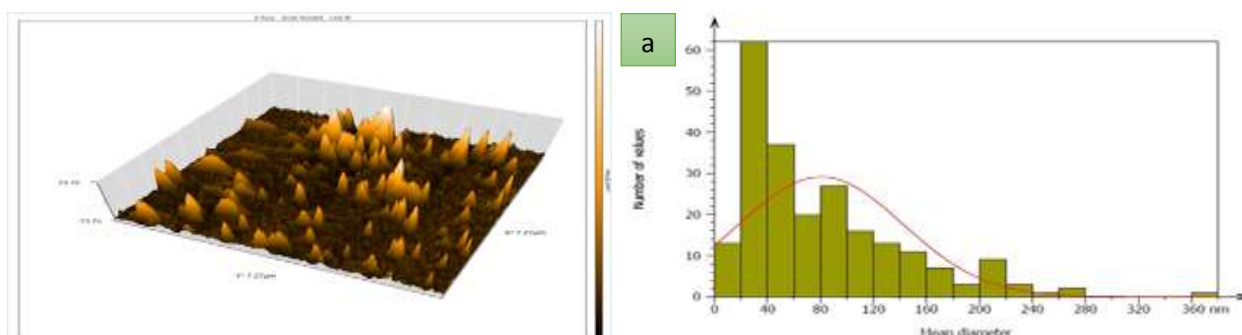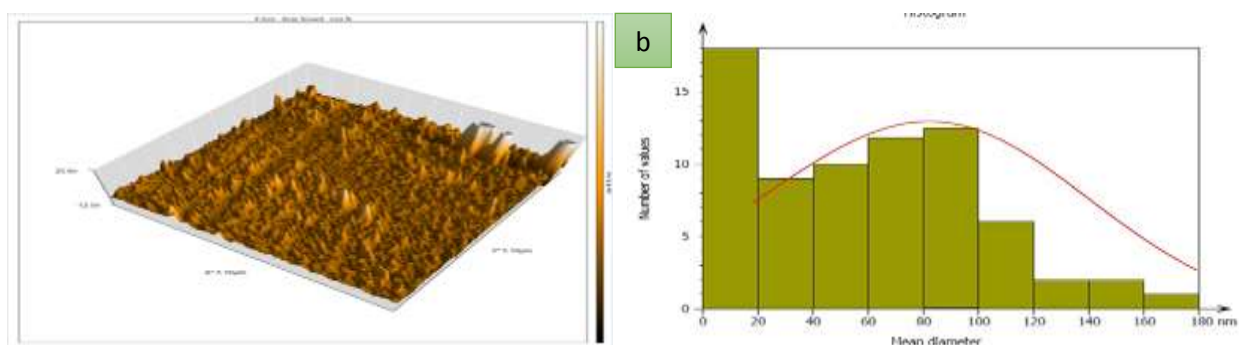
Figure 4. The 3D view of AFM image and granularity cumulating distribution chart of (a) NiO-P (b) NiO-G.

3.1.4 Scanning electron microscopy (SEM) analysis

The SEM analysis shows the crystalline structure, size of NPs, and porosity of the surface. **Figure 5** demonstrates the SEM **Image** for NiO−NPs samples. The average particle sizes calculated using the **Image J** software for NiO-P and NiO-G are 26.35 and 36.87 nm, respectively. Because of the phytochemicals present in the biosynthesized samples, which worked to produce the NPs, fill in gaps on the surfaces of NiO-NPs, and make the surface very porous, the morphology of NPs shows that they are various shapes with a rhombohedral cubic structure and aggregated into more spherical, irregular, and geometric shapes of varied sizes. These results agree with the study of Rashid *et al*., [21].
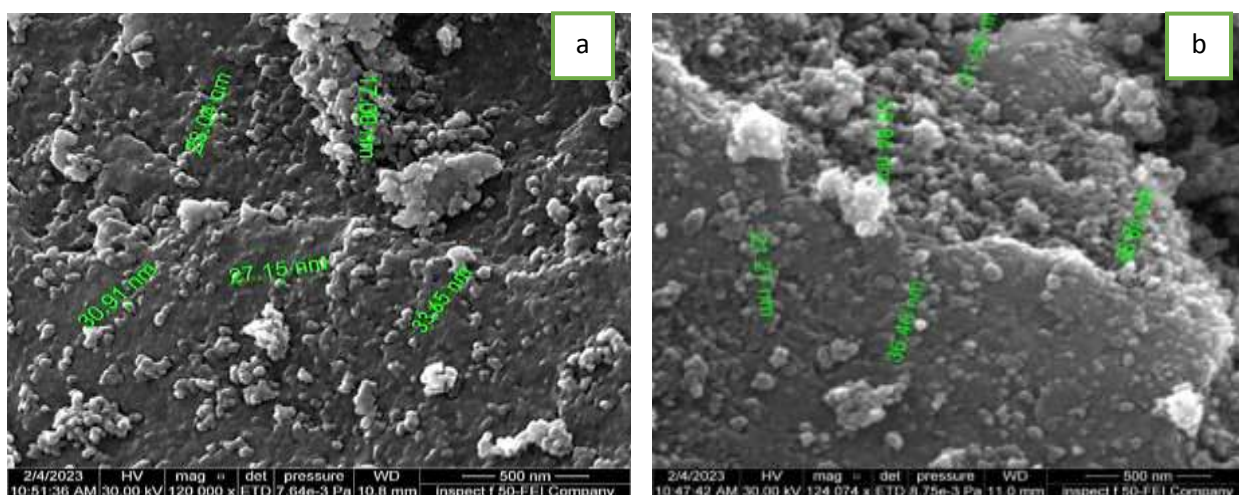
Figure 5. The SEM images for (a)NiO-P (b)NiO-G.

3.1.5 Brunauer–emmett–teller (BET) analysis

Figure 6 (a, b) shows the adsorption-desorption of N_2 gas at 77 K, which was used to predict the specific surface area and porosity information using the BET analysis [22]. The values of monolayer capacity V_m are found to be 14.286 and 9.7046 cm³/g, and the specific surface area (SBET) is 62.188 and 42.243 m²/g, while the mean pore diameter is 26.937 and 22.158 nm for NiO-P and NiO-G, respectively.
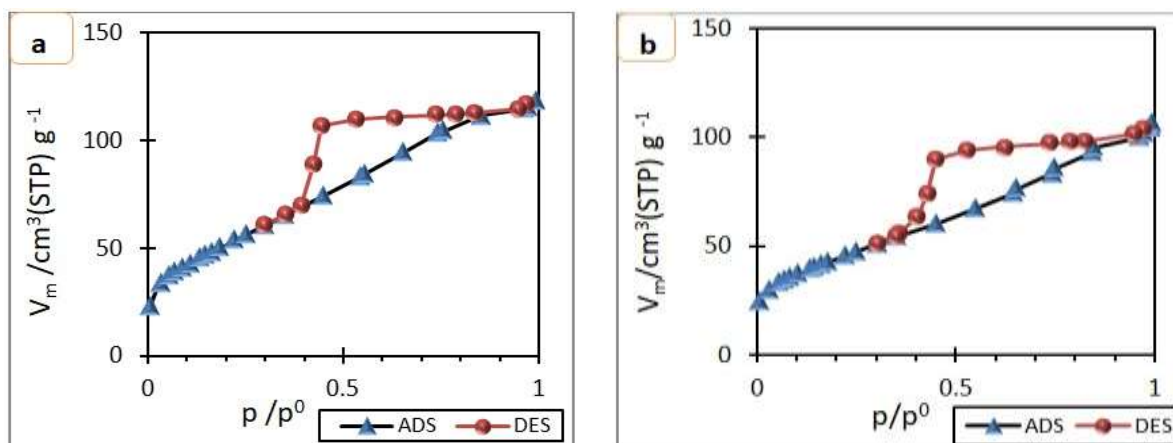
Figure 6. The N$_2$ gas adsorption-desorption isotherm for (a) NiO-P, (b) NiO-G samples at 77 K.

3.2 Optimization study for the adsorption conditions

3.2.1 Effect of initial concentration BS

Figure 7 (a,b) shows the impact of the initial BS concentration on the (a) removal percentage and (b) amount of adsorbed dye. As shown in **Figure 7(a)**, the removal percentage R% decreased from 94.22 and 81.75% to 74.64 and 62.17% for the samples NiO-P and NiO-G. When the sites on the surface of the adsorbent are occupied by the starting BS dye concentration, saturation is achieved at a lower dye concentration. Hence, by increasing the BS dye concentration, no further adsorption is achieved; as the concentration of BS increases, the amount of dye removed decreases [23]. While, **Figure 7(b)** shows an increase in the amount of adsorbed dye (qe) from 4.66 and 4.25 mg/g to 18.66 and 15.54 mg/g for NiO-P and NiO-G samples. The increase in the amount of adsorbed dye (qe) from 4.66 and 4.25 mg/g to 18.66 and 15.54 mg/g for NiO-P and NiO-G samples can be attributed to sorption becoming independent of starting BS concentration at a low ratio of available sites per unit dye concentration. As the dye concentration increased, more BS molecules became available per unit mass, gradually filling up the binding sites and resulting in higher qe values [24].
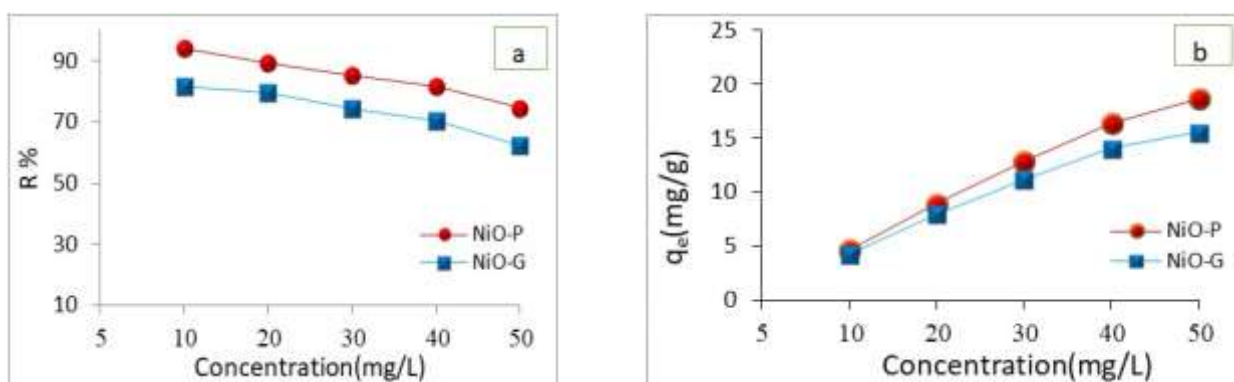
Figure 7. Impact of initial BS concentration on (a) Removal percentage (R%) (b) Amount of adsorbed dye.

3.2.2 Effect of NiO−NPs dosage

Figure 8 shows the effect of adsorbent dosage on the removal percentage R% of BS dye. It can be observed that with increasing the dosage of NiO−NPs, the values of R% increased from 56.80 and 48.48% to 94.22 and 84.86% for NiO-P and NiO-G samples, respectively. An optimal

weight of 0.05 g was selected for both samples. According to the findings, the number of active centers on the surface rises with increasing NiO-NP amounts [25].
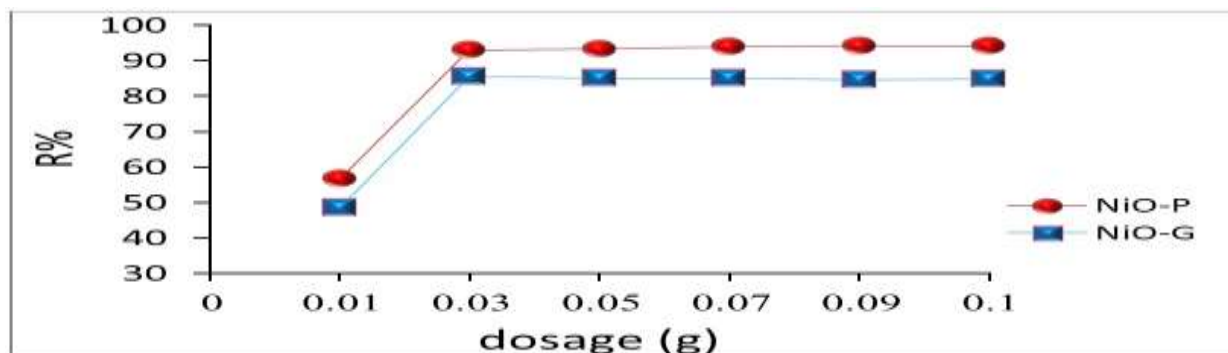
Figure 8. Impact of adsorbent weight on the R% of BS dye adsorption onto NiO-NPs samples.

3.2.3 Effect of contact time

Adsorption time impacts the removal efficiency of BS dye using NiO−NPs samples, as shown in **Figure 9**. The removal efficiency of BS dye increases as the adsorption time increases until it reaches the equilibrium time of 40 minutes. The rate of adsorption was observed to be slightly lower; this trend may be due to the accumulation of dye molecules onto available sites [26].
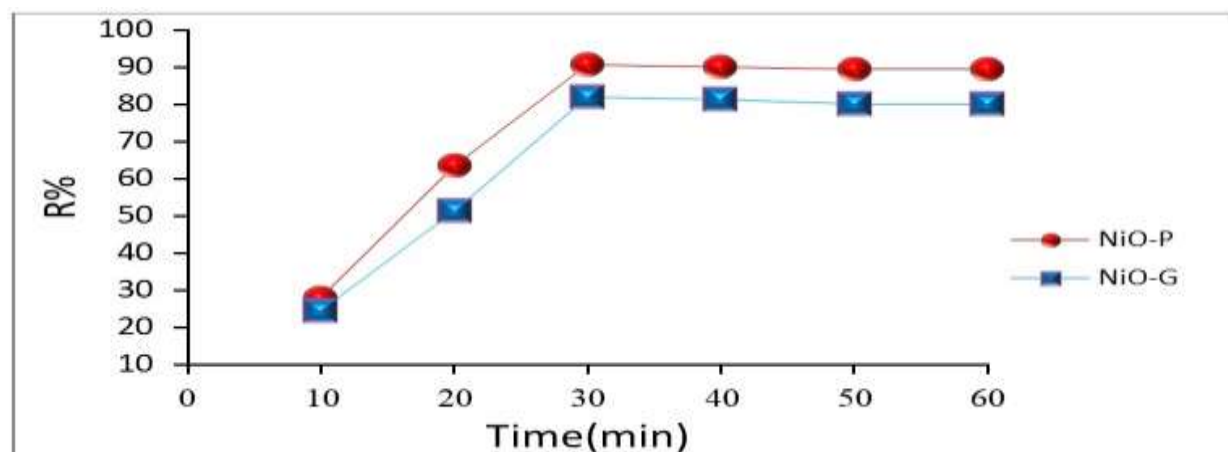
Figure 9. Influence of agitation time on the removal percentage of BS dye using NiO-NPs sample.

3.2.4 Effect of initial pH solutions

pH is the most critical factor affecting the adsorption of BS dye on the NiO−NPs samples. As shown in **Figure 10**, at pH higher than 7, the removal efficiencies of BS dye for NiO-P and NiO-G decreased from 99.3% to 98%77.2% and 96.2% to 65.8%, respectively. This is due to repulsion forces between the anionic BS dye and the NiO-NPs sample surface that were established, according to the presence of OH- ions, as shown in **Eq. 12**. In an acidic medium (**Eq. 13**), the electrostatic and ion-exchange activities between the BS dye and adsorbent surface increased at elevated pH, NiO particles have a positive surface charge, and high adsorption efficiency is anticipated because of the attraction forces between positive charged functional groups on the surface of NiO−NPs and the negatively charged surface of BS dye.

$$\text{Ni—OH} + \text{OH}^- \longrightarrow \text{Ni—O}^- + \text{H}_2\text{O} \tag{12}$$

$$\text{Ni—OH} + \text{H}^+ \longrightarrow \text{NiOH}_2^+ \tag{13}$$
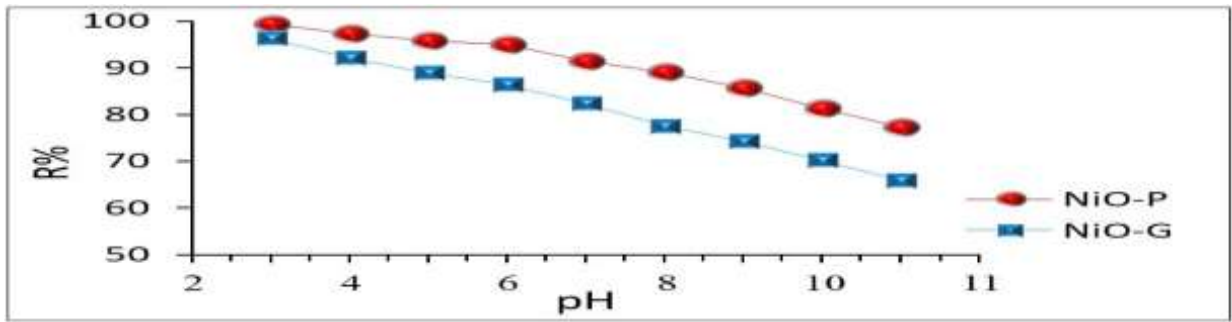
Figure 10. Impact of pH solution on the removal percentage of BS dye using NiO-NPs samples.

3.2.5 Influence of temperature solutions

The effect of temperature on dye removal efficiency was investigated by varying the temperatures from 293 K to 318 K while keeping other parameters constant. **Figure 11** shows that the removal efficiency increases with a rise in temperature. This may be related to the fact that both adsorption and absorption occur on the surfaces of the samples and that the sorption process is endothermic in nature [27].
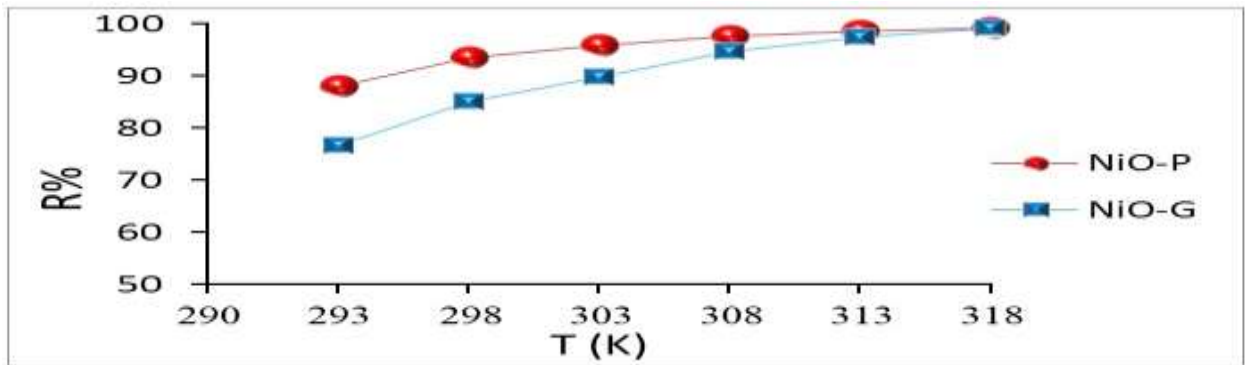
Figure 11. Influence of temperature on removal efficiency for BS dye using NiO−NPs samples.

3.3 Adsorption isotherm models
3.3.1 Langmuir isotherm model

The values of Langmuir constants qm and KL are obtained from the linear plot between Ce/qe versus Ce (**Eq. 3**), **Figure 12**. These values, along with the values of Rs, are represented in **Table 1**. From the values of Rs, it can be concluded that the Rs values between 0 and 1 $(0 < R_S < 1)$ indicate that the adsorption of BS dye onto NiO−NPs samples is favorable.
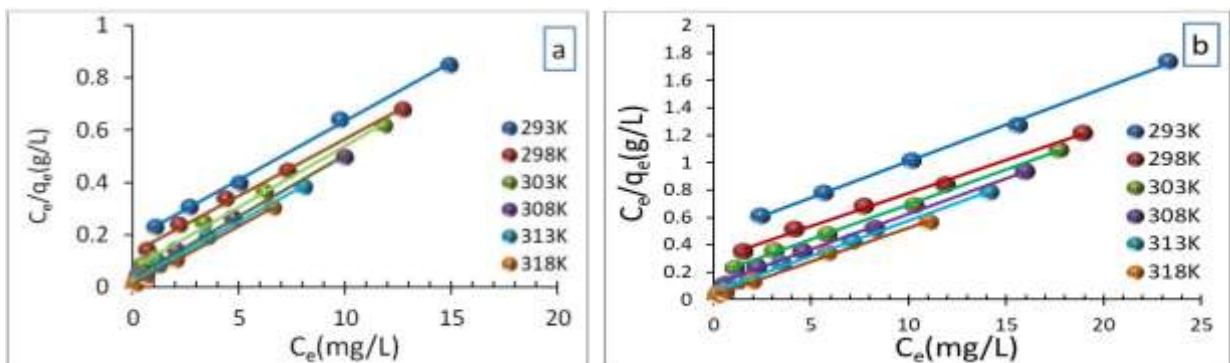
Figure 12. Langmuir isotherms model of BS dye adsorption onto: (a)NiO−P, (b) NiO-G.

Table 1. Langmuir constants for adsorption BS dye onto NiO−NPs samples at different temperatures.

Adsorbent	Temp (K)	q_m (mg/g)	K_L (L/mg)	R_s	R^2
NiO-P	293	25.069	0.1724	0.3671	0.9987
	298	23.423	0.3226	0.2366	0.9882
	303	23.269	0.5678	0.1497	0.9871
	308	24.364	0.7925	0.1120	0.9935
	313	26.653	0.9747	0.1143	0.9711
	318	26.314	1.5204	0.0610	0.9972
NiO-G	293	20.036	0.0830	0.5465	0.9982
	298	21.215	0.1244	0.4457	0.9732
	303	22.333	0.1709	0.3691	0.9655
	308	22.782	0.6713	0.1296	0.9911
	313	23.754	0.9276	0.0973	0.9687
	318	23.950	1.3514	0.0512	0.9689

The high values of monolayer capacity qm for NiO-P and NiO-G are related to the presence of active functional groups such as terpenoids, phenols, flavonoids, carbohydrates, and lignin compounds on the surfaces of NiO−NPs, which were synthesized by green methods. These particles have more pores, a smaller size, and a larger surface area. Our results agree with Al-Shammari *et al*., [28].

3.3.2 Freundlich isotherm model

Figure 13 depicts the linear plot between ln qe versus ln Ce (**Eq. 5**). The values of the Freundlich constants KFr and nf are listed in **Table 2**. It can be seen that the values of 1/nf < 1, indicate that the sorption of BS dye onto NiO-NPs samples is favorable.
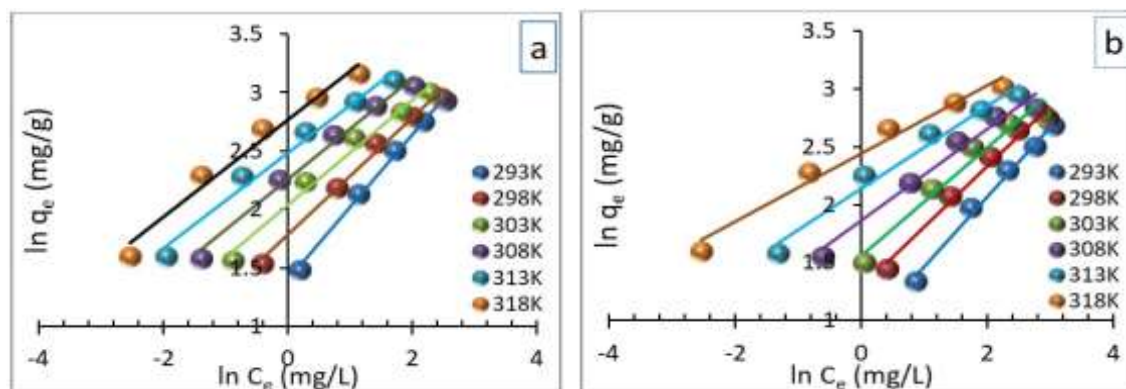
Figure 13. Freundlich isotherms plots for the adsorption of BS dye onto: (a) NiO−P, (b) NiO-G.

From the values of the correlation coefficient obtained for these two models, it can be noticed that the Langmuir model nearly explained the applicability of the adsorption data, and the adsorption of BS dye onto both adsorbents followed the mono-layer adsorption model.

Table 2. Freundlich isotherm constants for the adsorption of BS dye onto NiO−NPs samples at different temperatures.

Adsorbent	Temp. (K)	n_f	K_{Fr} $(mg/g(mg/L)^{-1/n})$	R^2
NiO−P	293	1.7575	4.2631	0.9236
	298	2.0638	6.0577	0.9637
	303	2.2878	8.0124	0.9663
	308	2.3244	9.6618	0.9834
	313	2.2096	10.599	0.9755
	318	2.2602	13.790	0.9701
NiO−G	293	1.6088	2.3599	0.9113
	298	1.7511	3.4477	0.9323
	303	2.0408	5.5769	0.954
	308	2.3775	8.4560	0.9601
	313	2.4324	10.471	0.9531
	318	2.4537	10.582	0.9658

3.4 Adsorption and thermodynamic parameters

Figure 14 shows the Van't Hoff plots between ln keq and 1/T (**Eq. 7**). The spontaneity of an adsorption process is greatly influenced by thermodynamic parameters, as shown in **Table 3**. As a result, the adsorption process was assumed to be spontaneous based on the negative values for the change in the Gibbes free energy ΔG^o at the specified temperature. However, the positive values for $\Delta H°$ suggested that the process was endothermic. This may be connected to the occurrence of the sorption process, which includes both adsorption and absorption. In addition, the positive ΔS^o values indicate increased randomness during this process [29]. These results are similar to those obtained by Kadhim *et al*., [30].
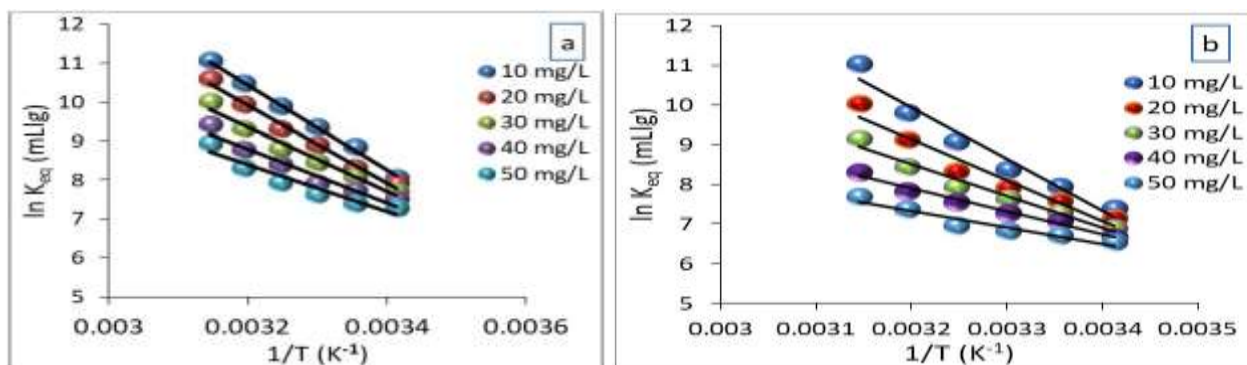
Figure 14. Van't Hoff plots adsorption of BS dye onto (a)NiO−P, (b) NiO-G at various temperatures.

Table 3. Thermodynamic parameters for the adsorption of BS dye onto NiO−NPs samples.

Adsorbent	C_i mg/L	$\Delta H°$ (kJ/mol)	$\Delta S°$ (J/mol.K)	$(-)\Delta G^o$ (kJ/mol) 293K	298K	303K	308K	313K	318K
NiO−P	10	73.715	320.66	19.989	21.958	23.586	25.345	26.536	28.079
	20	56.268	259.24	19.455	20.824	22.981	24.030	23.795	26.509
	30	64.219	282.36	18.577	19.999	21.299	22.571	23.964	25.85
	40	55.783	250.94	18.102	18.800	19.962	21.490	22.548	24.376
	50	45.377	213.88	17.392	18.352	19.357	20.364	21.523	22.794
NiO−G	10	90.024	368.55	18.021	19.709	21.267	24.114	25.338	24.960
	20	101.04	404.03	17.434	18.762	21.743	23.767	25.518	23.685
	30	103.46	408.48	16.936	18.046	19.632	22.159	23.848	23.354
	40	59.531	258.99	16.518	17.468	18.802	20.343	21.638	22.780
	50	65.897	278.89	15.951	17.226	18.476	19.677	21.677	22.223

3.5 Adsorption kinetics

3.5.1 Pseudo-first-order (PFO) model

Figure 15 shows the graph between ln (q_e-q_t) versus t (**Eq. 10**). The value of K_1, q_e, and R_2 are shown in **Table 4**.
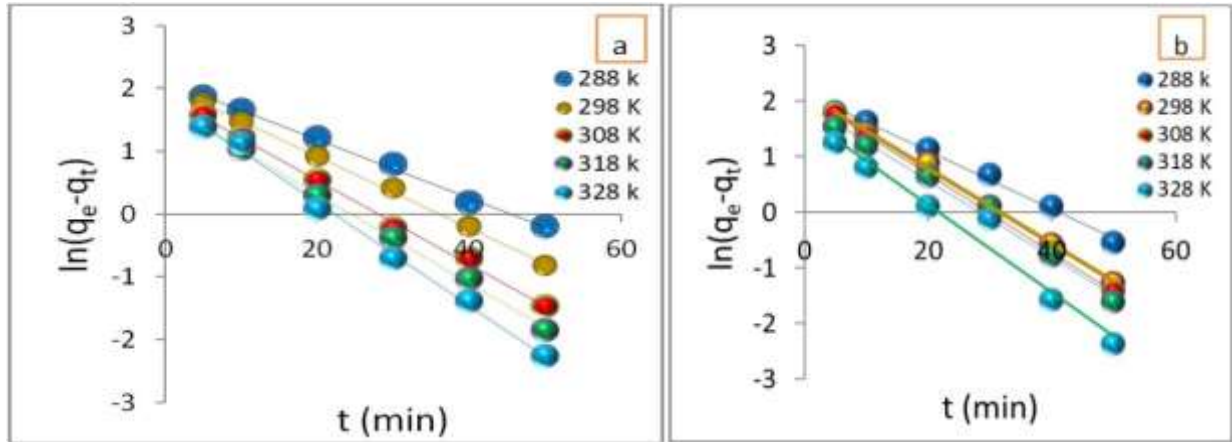
Figure 15. The PFO plots for the adsorption of BS dye onto(a)NiO-P,(b)NiO-G at different temperatures.

Table 4. Rate constants of PFO model for the adsorption of BS dye onto NiO−NPs samples.

Temp. (K)	NiO-P				NiO-G			
	$q_{e\ exp}$ (mg.g^{-1})	$q_{e\ cal}$ (mg.g^{-1})	k_1 (min^{-1})	R^2	$q_{e\ exp}$ (mg.g$_{-1}$)	$q_{e\ cal}$ (mg.g^{-1})	k_1 (min^{-1})	R^2
288	8.3389	4.2577	0.0379	0.8916	8.3493	6.3092	0.0407	0.8631
298	9.1705	6.0085	0.0489	0.9365	8.6507	5.7754	0.0453	0.9198
308	9.3680	6.4287	0.0668	0.9588	9.1705	5.1183	0.0462	0.9615
318	9.6071	5.7049	0.0708	0.9991	9.5135	5.0283	0.0542	0.9838
328	9.8669	6.4413	0.0820	0.9859	9.6175	5.4206	0.0675	0.9749

As shown in **Table 4**, the calculated qe cal values disagree with the experimental qe exp at different temperatures. Moreover, the values of the correlation coefficients (R_2) at 298K are 0.9365 and 0.9198 for NiO−P and NiO−G, respectively. It can be indicated that the PFO is not applicable adequately in this study.

3.5.2. Pseudo-second-order (PSO) model

Figure 16 shows the linear plot between t/q_t versus t (**Eq.11**), with the values of q_e, k_2 and R_2 listed in **Table 5**.
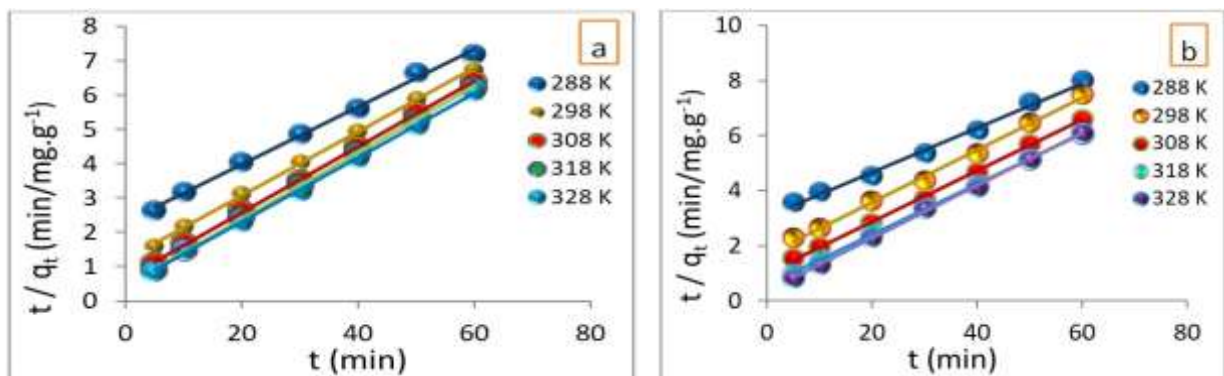
Figure 16. The PSO plots for adsorption of BS dye onto (a)NiO-P, (b)NiO-G at different temperatures.

Table 5. The PSO data for the adsorption of BS dye onto NiO−NPs samples at different temperatures.

Temp. (K)	NiO−P				NiO−G			
	$q_{e\ exp}$ (mg.g^{-1})	$q_{e\ cal}$ (mg.g^{-1})	k_2 (g/mg.min)	R^2	$q_{e\ exp}$ (mg.g^{-1})	$q_{e\ cal}$ (mg.g^{-1})	k_2 (g/mg.min)	R^2
288	8.3389	8.4082	0.0109	0.9762	8.3493	8.4048	0.0054	0.9408
298	9.1705	9.4950	0.0094	0.9841	8.6507	8.1005	0.0081	0.9722
308	9.3680	8.5290	0.0128	0.9956	9.1705	8.3027	0.0108	0.9915
318	9.6071	9.4600	0.0180	0.9957	9.5135	9.4699	0.0140	0.9962
328	9.8669	9.6800	0.0201	0.9971	9.6175	9.3609	0.0198	0.9966

It is clear from this table that the values of the correlation coefficient are in the range of 0.9762-0.9971 and 0.9408-0.9966 for NiO-P and NiO-G, respectively. Furthermore, the $q_{e\ cal}$ values are almost in agreement with the experimental $q_{e\ exp}$ at all temperatures. This indicates that the PSO is a better fit for the adsorption data than the PFO.

4. Conclusion

Green synthesis of NiO-NPs with Allium porrum and Apium graveolens plants produces NiO-P and NiO-G NPs with an excellent ability to remove BS dye from aqueous solutions. The Langmuir isotherm model fitted well with experimental data for the adsorption of BS onto the NiO-NPs samples. The synthesized NiO−NPs lead to enhanced values of monolayer capacity q_m due to the presence of phytochemical compounds in the NiO-NPs samples. According to the adsorption thermodynamic functions $\Delta G°$, $\Delta H°$, and $\Delta S°$, the adsorption is endothermic and occurs spontaneously. The results obtained through the kinetics study show that PSO is the best representation of adsorption kinetics. Overall, it was concluded that using plan extract provided an easy and cheap method for synthesizing NiO-NPs with a large specific surface area.

Conflict of Interest

The authors declare they have no competing interests.

Ethical Clearance

This work has been approved by the Institutional Scientific Committee at the University of Baghdad/ College of Sciences.

References

1. Ahmad, H.; Aziz, T.; Zia, M.; Sabir, M.; Khalid, H. Sources and composition of waste water: threats to plants and soil health. In *Soil Science: Agricultural and Environmental Prospectives*; *Springer* **2016**, 349-370. https://doi.org/10.1007/978-3-319-34451-5_16.
2. Cooksey, C. Quirks of dye nomenclature. 13. Biebrich scarlet. *Biotechnic & Histochemistry* **2020**, *95*, pp.194-197. https://doi.org/10.1080/10520295.2019.1662945.

3. Rashid, T.U.; Kabir, S.F.; Biswas, M.C.; Bhuiyan, M.R. Sustainable wastewater treatment via dye–surfactant interaction: a critical review. *Industrial & Engineering Chemistry Research* **2020**, *59*, 9719-9745. https://dx.doi.org/10.1021/acs.iecr.0c00676.

4. Al Nasir, H.; Mohammed, S. Experimental investigation on adsorption of methyl orange using eggshells as adsorbent surface. *Ibn AL-Haitham Journal For Pure and Applied Sciences* **2023**, *36*(*1*), 197-207. https://doi.org/10.30526/36.1.2890.

5. Foroutan, R.; Mohammadi, R.; Farjadfard, S.; Esmaeili, H.; Saberi, M.; Sahebi, S.; Dobaradaran, S.; Ramavandi, B. Characteristics and performance of Cd, Ni, and Pb bio-adsorption using callinectes sapidus biomass: real wastewater treatment. *Environmental Science and Pollution Research* **2019**, *26(7)*,6336-6347. https://doi.org/10.1007/s11356-018-04108-8.

6. Rivero-Montejo, S.; Vargas H.; Torres-Pacheco, I. Nanoparticles as Novel Elicitors to Improve Bioactive Compounds in Plants. *Agriculture* **2021**, *11(2)*,134. https://doi.org/10.3390/agriculture11020134.

7. Hadi, K.; Al- Saadi, T. Investigating the structural and magnetic properties of nickel oxide nanoparticles prepared by precipitation method. *Ibn AL-Haitham Journal For Pure and Applied Sciences* **2022**, *35(4)*,94-103. https://doi.org/10.30526/35.4.2872.

8. Abdul-Ameer, Z. Novel Co-Precipitation method for synthesis of nanostructured nickel oxide in accordance to PH: Structural and optical properties as an active optical filter. *Ibn AL-Haitham Journal For Pure and Applied Sciences* **2019**, *32(1)*,1-6. https://doi.org/10.30526/32.1.1974.

9. Onukwuli, O.; Obiora-Okafo, I.; Omotioma, M. Characterization and colour removal from an aqueous solution using bio-coagulants: response surface methodological approach. *Journal of Chemical Technology &Metallurgy* **2019**, *54(1)*,77-89.https://journal.uctm.edu/node/j2019-1/1017198p7789.pdf.

10. Aziz, W.; Abd Urabe, A. Chemical preparation of iron oxide nanoparticles using plants extracts in antibacterial application. *International Journal of Bioorganic Chemistry* **2019**, *4(1)*,1. https://doi.org/10.11648/j.ijbc.20190401.11.

11. Huang, Z.; Li, Y.; Chen, W.; Shi, J.; Zhang, N.; Wang, X.; Li, Z.; Gao, L.; Zhang, Y. Modified bentonite adsorption of organic pollutants of dye wastewater. *Materials Chemistry and Physics* **2017**, *202*, 266-276. https://doi.org/10.1016/j.matchemphys.2017.09.028.

12. Al-Saade KAS, AL-Mammar DE, AL-Ani HN. Using phragmites australis (Iraqi plant) to remove the lead (II) ions form aqueous solution. *Baghdad Science Journal* **2017**, *14(1)*,0148. https://doi.org/10.21123/bsj.2017.14.1.0148.

13. Abbas, A.M.; Mohammed, Y.I.; Himdan, T.A. Adsorption of anionic dye from equeous solution by modified synthetic zeolite. *Ibn AL-Haitham Journal For Pure and Applied Sciences* **2017**, *28(2)*, 52-68. https://jih.uobaghdad.edu.iq/index.php/j/article/view/177.

14. Mushtaq, M.; Bhatti, H.; Iqbal, M.; Noreen, S. Eriobotrya japonica seed biocomposite efficiency for copper adsorption: Isotherms, kinetics, thermodynamic and desorption studies. *Journal of Environmental Management* **2016**, *176(7)*, 21-33. https://doi.org/10.1016/j.jenvman.2016.03.013.

15. Lima, E.; Gomes, A.; Tran, H. Comparison of the nonlinear and linear forms of the van't Hoff equation for calculation of adsorption thermodynamic parameters ($\Delta S°$ and $\Delta H°$). *Journal of Molecular Liquids* **2020**, *311*,113315. https://doi.org/10.1016/j.molliq.2020.113315.

16. Liu, L.; Luo, X.; Ding, L.; Luo, S. Application of nanotechnology in the removal of heavy metal from water. In nanomaterials for the removal of pollutants and resource reutilization, *Elsevier* **2019**, 83-147. https://doi.org/10.1016/B978-0-12-814837-2.00004-4.

17. Yuh-Shan, H. Citation review of Lagergren kinetic rate equation on adsorption reactions. *Scientometrics* **2004**, *59(1)*,171-177. https://doi.org/10.1023/b:scie.0000013305.99473.cf.

18. Saxena, M.; Sharma, N.; Saxena, R. Highly efficient and rapid removal of a toxic dye: adsorption kinetics, isotherm, and mechanism studies on functionalized multiwalled carbon nanotubes. *Surfaces and Interfaces* **2020**, *21(2018)*,100639. https://doi.org/10.1016/j.surfin.2020.100639.

19. Ho, Y. Using of pseudo-second-order model in adsorption. *Environmental Science and Pollution Research* **2014**, *21(11)*,7234-7235. https://doi.org/10.1007/s11356-013-2213-9.

20. Sabouri, Z.; Akbari, A.; Hosseini, H.; Darroudi, M. Facile green synthesis of NiO nanoparticles and investigation of dye degradation and cytotoxicity effects. *Journal of Molecular Structure* **2018**, *1173*, 931-936. https://doi.org/10.1016/j.molstruc.2018.07.063.

21. Rashid, I.; Salman, S.; Kareem Mohammed, P.; Mahdi, Y. Green synthesis of nickle oxide nanoparticles for adsorption of dyes. *Sains Malaysiana* **2022**, *51(2)*,533-546. https://doi.org/ 10.17576/jsm-2022-5102-17.

22. Zheng, Y.; Zhu, B.; Chen, H.; You, W.; Jiang, C.; Yu, J. Hierarchical flower-like nickel (II) oxide microspheres with high adsorption capacity of Congo red in water. *Journal of Colloid and Interface Science* **2017**, *504*, 688-696. http://dx.doi.org/10.1016/j.jcis.2017.06.014.

23. Omar S.; Dunya E. Adsorption of Biebrich scarlet dye onto nano NiO and modified nano NiO: Isotherms, thermodynamic and kinetic studies. *Journal of Survey in Fisheries Sciences* **2023**, *10(3S)* 3432-3441. https://doi.org/10.17762/sfs.v10i3S.1195.

24. Sonawane, S.; Chaudhari, P.; Ghodke, S.; Phadtare, S.; Meshram, S. Ultrasound assisted adsorption of basic dye onto organically modified bentonite (nanoclay). *Journal of Scientific & Industrial Rese* **2009**, *68(2)*,162-167. http://nopr.niscpr.res.in/handle/123456789/2915.

25. Khan, N.; Saeed, K.; Khan, I.; Gul, T.; Sadiq, M.; Khan, A.; Zekker, I. Efficient photodegradation of orange II dye by nickel oxide nanoparticles and nanoclay supported nickel oxide nanocomposite. *Applied Water Science* **2022**, *12(131)*,375-654. https://doi.org/10.1007/s13201-022-01647-x.

26. Pandian, C.; Palanivel, R.; Dhananasekaran, S. Green synthesis of nickel nanoparticles using Ocimum sanctum and their application in dye and pollutant adsorption. *Chinese Journal of Chemical Engineering* **2015**, *23(8)*,1307-1315. https://doi.org/10.1016/j.cjche.2015.05.012.

27. Sabouri, Z.; Akbari, A.; Hosseini, H.A.; Hashemzadeh, A.; Darroudi, M. Bio-based synthesized NiO nanoparticles and evaluation of their cellular toxicity and wastewater treatment effects. *Journal of Molecular Structure* **2019**, *119(1)*,101-109. https://doi.org/10.1016/j.molstruc.2019.04.075.

28. Al-Shammari, N.; Al-Mammar, D. Adsorption of Biebrich Scarlet Dye into Remains Chromium and Vegetable Tanned Leather as Adsorbents. *Iraqi Journal of Science* **2022**, *63(7)*,2814-2826. https://doi.org/10.24996/ijs.2022.63.7.6.

29. Al-Ghouti, M.; Da'ana, D. Guidelines for the use and interpretation of adsorption isotherm models: A review. *Journal of hazardous materials* **2020**, *393*,122383. https://doi.org/10.1016/j.jhazmat.2020.122383.

30. Kadhim, H.; Saleh, K. Removing cobalt ions from industrial wastewater using chitosan. *Iraqi Journal of Science* **2022**, *63(8)*,3251-3263. https://doi.org/10.24996/ijs.2022.63.8.1.